

# Geometrical properties of mechanically annealed systems near the jamming transition

Hiromichi Matsuyama<sup>a,1</sup>, Mari Toyoda<sup>1</sup>, Takumi Kurahashi<sup>1</sup>, Atsushi Ikeda<sup>2</sup>, Takeshi Kawasaki<sup>1</sup>, Kunimasa Miyazaki<sup>b,1</sup>

<sup>1</sup>Department of Physics, Nagoya University, Nagoya 464-8602, Japan

<sup>2</sup>Graduate School of Arts and Sciences, University of Tokyo, Tokyo 153-8902, Japan

Received: date / Accepted: date

**Abstract** Geometrical properties of two-dimensional mixtures near the jamming transition point are numerically investigated using harmonic particles under mechanical training. The configurations generated by the quasi-static compression and oscillatory shear deformations exhibit anomalous suppression of the density fluctuations, known as hyperuniformity, below and above the jamming transition. For the jammed system trained by compression above the transition point, the hyperuniformity exponent increases. For the system below the transition point under oscillatory shear, the hyperuniformity exponent also increases until the shear amplitude reaches the threshold value. The threshold value matches with the transition point from the point-reversible phase where the particles experience no collision to the loop-reversible phase where the particles' displacements are non-affine during a shear-cycle before coming back to an original position. The results demonstrated in this paper are explained in terms of neither of universal criticality of the jamming transition nor the nonequilibrium phase transitions.

## 1 Introduction

As the density of athermal soft particles is increased, the system stops flowing and attains rigidity at some point. This is called the jamming transition [1–3]. In the last decade, we witnessed tremendous progress in our understanding of the jamming transition of frictionless particle systems, driven by the development of the mean-field theory and extensive numerical/experimental studies [4–6]. It is now well established that power-law behaviors of observables such as the contact number, shear/bulk modulus, the radial distributions are independent of spatial dimensions, as long as the constituent particles are spherical [3, 7]. The critical behaviors are also observed in the vibrational and rheological behavior of the systems [8–16]. Moreover, the argument is now extended to non-spherical particles systems [17]. These results support the universal class of the jamming transition and bolster the success of the mean-field theory.

There are, however, some properties that still elude the explanation in terms of the mean-field theory and the universal criticality. One of them is an anomalous suppression of the density fluctuations called hyperuniformity [18, 19]. Originally suggested in the fluctuations of the early universe [20], hyperuniformity is observed in a variety of systems such as avian photo-receptor cells [21], active matters [22], and dilute colloidal suspensions under oscillatory shear [23, 24]. The jammed particles system is among the first examples which exhibit hyperuniformity [25].

Hyperuniformity is a new type of long-range correlation characterized by the suppression of the static structure factor or the  $q$ -dependent compressibility,  $\chi(q)$ , where  $q$  is the wavevector. The system is said to be hyperuniform if  $\chi(q)$  vanishes as  $q^\alpha$  with a positive exponent  $\alpha$  instead of  $\alpha = 0$ . Equivalently, the hyperuniformity is defined by the suppression of the local density fluctuations  $\sigma_\rho^2(R) \equiv \langle \delta\rho^2(R) \rangle$ , where  $\delta\rho(R)$  is the density fluctuations inside an observation window of the radius  $R$  [19]. For hyperuniform systems,  $\sigma_\rho^2(R)$  decreases as  $R^{-\beta}$  ( $\beta > d$ ) where  $d$  is the spatial dimension. This is faster than  $R^{-d}$  for equilibrium liquids. The exponent  $\beta$  is related to  $\alpha$  by  $\beta = d + \alpha$ , if

<sup>a</sup>e-mail: matsuyama@r.phys.nagoya-u.ac.jp

<sup>b</sup>e-mail: miyazaki@r.phys.nagoya-u.ac.jp

$\alpha \leq 1$  [19]. Hyperuniformity was presumed to be another sign of the jamming criticality but the power-law behavior of  $\chi(q) \sim q^\alpha$  is observed only in the finite range of the wavevector windows [26, 27]. It is argued that  $\chi(q)$  becomes strictly zero only when the jamming configuration is prepared from the ideally close-packed amorphous state (or the ideal glass state) [28]. However, a numerical study on the jamming configurations generated by quenching thermally annealed supercooled fluids shows that hyperuniformity is not enhanced [5]. Distinct but related jammed system of confluent living tissues also show hyperuniformity, but it has been discussed that hyperuniformity is not directly related to the fluid-solid transition [29]. Recently, hyperuniformity was also observed in the inherent structures of supercooled liquids [30] and in the frictional jammed systems [31].

In this paper, we numerically study the geometrical properties, with a special emphasis on hyperuniformity, of particle configurations near and below the jamming transition point under several mechanical training protocols. One protocol is the isotropic compression in which an unjammed configuration is compressed quasi-statically and isotropically up to a maximal density  $\varphi_{\text{MAX}}$  above the jamming transition point and then decompressed again until the pressure or the energy vanishes [32]. We define the jamming transition point  $\varphi_{J0}$ , as the value at which the pressure/energy becomes finite on the way of compression. As reported in Ref. [32], the jamming density at which the pressure/energy vanishes during the decompression, which we denote as  $\varphi_J$ , is larger than  $\varphi_{J0}$  and depends mildly on the amplitude of the compression cycle  $\varphi_{\text{MAX}}$ . This means that the jammed configuration is trained and the system finds more efficient packing during this mechanical cycle, much the same way as the jamming density increases as the parent fluid before quenching to generate the jamming configuration is equilibrated at lower temperatures [5, 33, 34]. For this reason, we use the word “training” for the same meaning as “annealing” in this paper. We investigate the density fluctuations of the jammed configurations at  $\varphi_J$  after one compression-decompression cycle.

Another system we study is the configurations slightly below  $\varphi_{J0}$  which is subject to quasi-static oscillatory shear. For a given configuration, we apply a quasi-static shear deformation cycle with a small amplitude. The cycles are applied until the system reaches the steady state and then we monitor the density fluctuations. The Poissonian-like large density fluctuations are suppressed quickly as the training shear amplitudes increase. In both systems, we find that the mechanical training enhances the hyperuniformity of the system.

This paper is organized as follows. After describing the method and the detail of the system which we study in Section 2, we first revisit hyperuniformity of a two-dimensional jammed configuration generated in the vicinity of the jamming transition point of the poorly trained system in Section 3. In Section 4, we analyze the rattler populations and hyperuniformity for the system generated by the compression training. We analyze hyperuniformity for the unjammed configurations under oscillatory shear in Section 5. We conclude this paper in Section 6.

## 2 Method and Model

The system we study is a two-dimensional equimolar binary mixture of frictionless particles with diameters  $\sigma_L$  and  $\sigma_S$  placed in a square box with periodic boundary conditions. The size ratio of small and large particles is  $\sigma_L/\sigma_S = 1.4$ . The particles interact with the harmonic potential defined by

$$U(r_{ij}) = \frac{\varepsilon}{2} \{1 - (r_{ij}/\sigma_{ij})\}^2, \quad (1)$$

if the inter-particle distance of the  $i$ -th and  $j$ -th particles is  $r_{ij} < \sigma_{ij}$  and 0 otherwise. Here  $\sigma_{ij} = (\sigma_i + \sigma_j)/2$  is the average diameter of the  $i$ -th and  $j$ -th particles. We use  $\sigma_S$ ,  $\varepsilon$ , and  $\varepsilon/k_B$  as the units of length, energy, and temperature, respectively.

For all simulations presented in this paper, we first generate jammed or unjammed configuration by quenching the random configuration at  $T = \infty$  to  $T = 0$  at a target volume fraction  $\varphi$ . For both mechanical compression (Section 4) and the oscillatory shear (Section 5), the configuration is optimized using the FIRE algorithm [35] for every infinitesimal step of the deformation. The number of samples is from 300 to 900. The details of the numerical method for the different protocols are given in each section.

## 3 Hyperuniformity of the poorly trained system

In this section, we revisit hyperuniformity of the poorly trained jammed configuration. Hyperuniformity in the vicinity of the jamming transition point  $\varphi_J$  is well documented for both two [36, 37] and three dimensional systems [5, 25–27, 38], but the properties of the hyperuniform configurations in two-dimensional systems have not been fully explored.

We generate the jamming configuration using the same method as in previous studies [33, 39]. The initial random particle configuration prepared at  $\varphi_{\text{ini}} =$

0.835 is quasi-statically compressed by an incremental small density  $\Delta\varphi = 10^{-5}$  up to the maximum density  $\varphi_{\text{MAX}} = 0.845$ . At every compression step, the system is stabilized using the FIRE algorithm [35]. When the density reaches  $\varphi_{\text{MAX}}$ , the system is decompressed with the step of  $\Delta\varphi$ . We monitor the energy  $E$  at every step and we judge the system is unjammed if the energy per one particle  $e = E/N$  becomes smaller than  $e = 10^{-16}$ . We determine the jamming transition point  $\varphi_J$  as the first density at which the system is unjammed during the decompression steps. We obtain the mean value of the jamming transition point  $\varphi_J = 0.842$ . In the analysis below, we monitor the density fluctuations at the jamming transition point of each sample. Throughout this section, the system size is  $N = 3000$  and we take the ensemble average over the 300 samples.

We use the wavevector-dependent compressibility  $\chi(q)$  to monitor the density fluctuations. For binary mixtures,  $\chi(q)$  is defined by

$$\chi(q) = \frac{S_{SS}(q)S_{LL}(q) - S_{LS}^2(q)}{x_S^2 S_{LL}(q) + x_L^2 S_{SS}(q) - 2x_S x_L S_{LS}(q)}, \quad (2)$$

where  $x_S = x_L = 1/2$  is the molar fraction of the small and large particles,  $S_{\nu\mu}(q) = \langle \delta\rho_\nu(q) \delta\rho_\mu^*(q) \rangle / N$  ( $\nu, \mu = S, L$ ) is the static structure factor matrix for the binary mixture [38]. Note that the small wavevector limit of  $\chi(q)$  is related to an isothermal compressibility by  $\chi(q \rightarrow 0) = \rho k_B T \chi_T$  in equilibrium. It is established that  $\chi(q)$  is a better observable to detect the hyperuniformity than the total structure factor  $S(q) = \sum_{\nu\mu=S,L} S_{\nu\mu}(q)$  [38]<sup>1</sup>. Recently, several variants of  $\chi(q)$  have been proposed [36], such as the local volume fraction correlation functions. The wavevector windows where hyperuniformity is observed vary depending on the variants but the long-length (small  $q$ ) behavior is insensitive to the definition [36].

In Figure 1, we show  $\chi(q)$  at  $\varphi_J$ .  $\chi(q)$  develops the power law region in the intermediate window of  $0.3 \lesssim q \lesssim 1.3$ , as it is the case for the three dimensional systems [5, 25–27, 38]. This algebraic behavior is not observed in the small- $q$  limit and  $\chi(q)$  bends up around  $q_{\text{HU}} \lesssim 0.3$ . This means that the system is not rigorously hyperuniform and the spatial correlation persists only up to a length scale  $q_{\text{HU}}^{-1}$ . We shall refer to  $q_{\text{HU}}^{-1}$  as the hyperuniform length. In the intermediate region,  $\chi(q)$  is fitted well by  $\chi(q) \sim q^\alpha$  with an exponent  $\alpha = 0.626 \pm 0.012$ , where we use the least square for fitting. This exponent is far smaller than  $\alpha \approx 1$

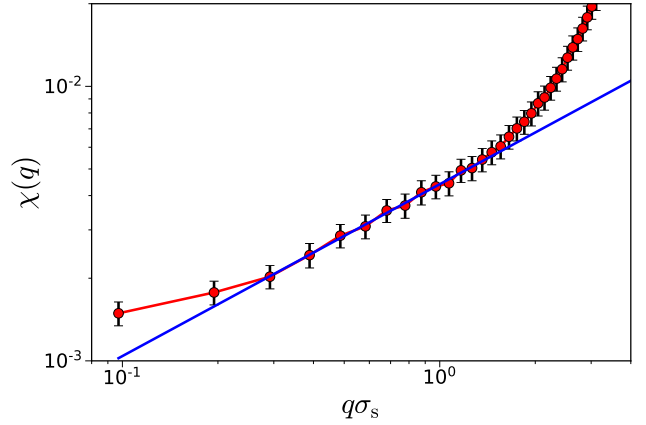


**Fig. 1**  $\chi(q)$  at  $\varphi_J$  for the poorly trained system. The red circles are simulation results with standard errors. The blue solid line is the power-law fit by  $\chi(q) \sim q^\alpha$  with the exponent  $\alpha = 0.626 \pm 0.012$ . The fitting was made in the window of  $0.3 \lesssim q \lesssim 1.3$ . The value of  $\alpha$  is smaller than  $\alpha \approx 1$  which is reported in previous study in three dimensional system.

for the three-dimensional systems. It may sound surprising because  $\alpha \approx 1$  were univocally reported in the literature on hyperuniformity of the jammed systems, irrespective of the spatial dimension. However, this result is not new. Although it has not been explicitly acknowledged in the previous studies [36, 37, 40], close inspection of the data shows that the values of exponents reported for the two-dimensional systems are consistent with ours. We check that the value of  $\alpha$  does not depend on the definition of  $\chi(q)$ . Several types of  $\chi(q)$  defined by different metrics have been proposed and studied recently [36, 38, 41]. Here we examine three definitions of  $\chi(q)$ 's introduced in Ref. [36]. Definition I [42]:  $\chi_I(q) \sim \langle |\Delta(q)|^2 \rangle$ , where  $\Delta(q)$  is the Fourier transformation of the local volume fraction defined by  $\sum_i \Delta_i(\mathbf{r} - \mathbf{r}_i)$  where  $\Delta_i$  is the step function which is 1 if  $\mathbf{r}$  is sitting inside the  $i$ -th disc at  $\mathbf{r}_i$  and 0 otherwise. Definition II [38]:  $\chi_{II}(q) \sim \langle |\delta\varphi(q)|^2 \rangle$ , where  $\delta\varphi(q)$  is the Fourier transformation  $\varphi(\mathbf{r}) = \sum_i v_i \delta_i(\mathbf{r} - \mathbf{r}_i)$  where  $v_i$  is of the area of the  $i$ -th disc. Definition III [38] is the  $q$ -dependent compressibility defined by (2). We show these three  $\chi(q)$ 's in Figure 2. Three  $\chi(q)$ 's match in the small  $q$  region with the identical power-law exponent. Although the width of window over which the power-law is observed varies depending on the definition and the shape at large  $q$ 's are salient, it is evident that the hyperuniform behaviors are robust irrespective of the choice of metrics.

The smaller exponent of  $\alpha \approx 0.6$  may be understood by recalling that the upper critical dimension of the jamming transition is 2. Let us consider an ideally hyperuniform jammed configuration. Then, the fluctuations  $\sigma_\phi^2(R) \equiv \langle \delta\phi^2 \rangle$  of a subsystem of the size  $R$  should

<sup>1</sup>In the ensemble-averaging of  $\chi(q)$ , we expand the system slightly to fix the simulation box-size for every sample. This is necessary since each sample jams at different volume fractions. We carefully checked that the effect of the small variation of the system size is negligible.

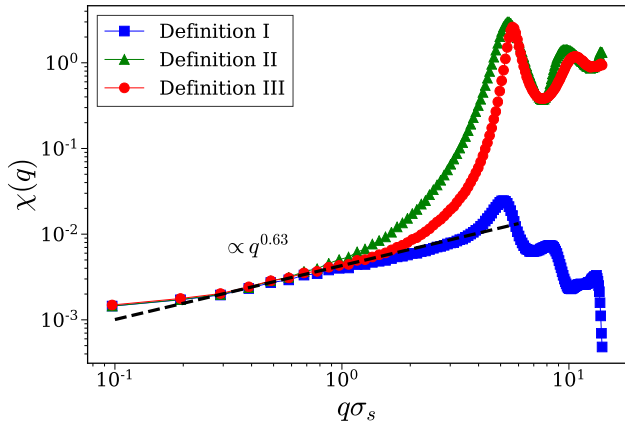


**Fig. 2**  $\chi(q)$  computed using three different definitions (see the text). Definition III is identical with that shown in Figure 1. The line of  $q^{0.63}$  is guide for eyes.

be scaled as  $R^{-d-\alpha}$  in the large  $R$  limit and its Fourier representation should behave as  $\chi_\phi(q) \sim q^\alpha$  [19]. Here  $\phi$  is a metric such as number density. On the other hand, the mean-field theory claims that  $\sigma_\phi^2(R) \sim N^{-\omega}$  should be scaled by  $N$  rather than  $R$  in the large  $N$  (or  $R$ ) limit [43, 44], where  $\omega$  is a dimension-independent exponent. Comparing the two expressions, one concludes  $d + \alpha = d\omega$ , or  $\alpha \propto d$ . Therefore, if  $\alpha = 1$  for  $d = 3$  as it is established, we should expect  $\alpha = 2/3 \approx 0.6$  for  $d = 2$ . Of course, this argument applies in the large  $N$  limit and in the ideally hyperuniform system. In the finite system, the scaling behavior of the real-space representation of the fluctuations  $\sigma_\phi^2(R)$  is polluted by, for example, the shape effect of subsystems [27] and, in realistic jammed systems,  $\chi_\phi(q) \sim q^\alpha$  breaks down below  $q_{\text{HU}}$ . However,  $\chi_\phi(q) \sim q^\alpha$  would survive in the intermediate window  $q > q_{\text{HU}}$  and should be less sensitive to the finite size effect.

The exponent of  $\alpha \approx 0.63$  are also observed in the system under nonequilibrium setting as we shall demonstrate in the following sections.

#### 4 Mechanically trained systems by the compression and decompression cycle

In this section, we investigate the jammed system under mechanical training by applying the compression-decompression cycle to the system. Kumar *et al.* has shown that, if a system jammed at a value of  $\varphi_{J0}$  is compressed by a certain amount up to  $\varphi_{\text{MAX}}$  and then decompressed, the system is unjammed at a value  $\varphi_J$  which is slightly larger than  $\varphi_{J0}$  [32]. If the compression-decompression cycle is applied multiple times,  $\varphi_J$  increases more. In other words, the jamming transition point  $\varphi_J$  shifts to a larger value as the system is trained

mechanically by compression. This is analogous to the thermal annealing effect in which  $\varphi_J$  increases if the parent fluid before quenching to generate the jammed packing is equilibrated at lower temperatures [33, 34]. Here we investigate how the geometrical properties of the jammed configurations change by such mechanical training. For thermal annealed systems for which the system parameters are carefully calibrated to facilitate the equilibration at high densities, it has been shown that (i) the number of rattlers increases substantially and (ii) concomitantly, hyperuniformity is mitigated as the system is more annealed [5]. It is somewhat counter-intuitive as we would naively expect that more stabilized and optimized amorphous configurations by annealing would prefer the fewer particles with no contacts and also would exhibit stronger hyperuniformity as the configurations are closer to those of the ideal glass [28].

We train the system mechanically using a quasi-static volume compression-decompression for one cycle using the protocol employed by Kumar *et al.* [32]. As explained in the previous section, the initial configuration prepared at  $\varphi_{\text{ini}} = 0.835$  slightly below  $\varphi_J$  is quasi-statically compressed to a maximum density  $\varphi_{\text{MAX}}$  with the step size of  $\Delta\varphi = 10^{-5}$ . As the density reaches  $\varphi_{\text{MAX}}$ , the system is decompressed with the same step size. We identify  $\varphi_J$  as the point where the energy per one particle  $e = E/N$  becomes smaller than  $e = 10^{-16}$ . For the analysis of the rattlers, we use the system size  $N = 1000$  and average over 600 samples. For the analysis of hyperuniformity,  $N = 3000$  and the number of samples is 300. The typical behavior of  $e$  during this compression cycle is shown in Figure 3. We simulate various values of  $\varphi_{\text{MAX}}$  ranging from 0.845 up to 1.3.

##### 4.1 Rattlers

Before discussing hyperuniformity, we comment on the change in the number of rattlers under mechanical training. It is documented that the jammed configurations generated from thermally annealed fluid which is equilibrated at a temperature well below the so-called onset temperature of the supercooled state tend to generate more rattlers than the jammed configurations generated by fast quench from the high-temperature fluids (or random configuration) [5]. We investigate if this counter-intuitive result holds for the jammed configurations under the mechanical training.

As reported in Refs. [32, 39],  $\varphi_J$  is a function of  $\varphi_{\text{MAX}}$  and increases slowly with  $\varphi_{\text{MAX}}$  (see Figure 4 (a)).  $\varphi_J$  sharply increases up to  $\varphi_{\text{MAX}} = 1$  and then saturate at slightly below 0.847 (the blue filled circles).

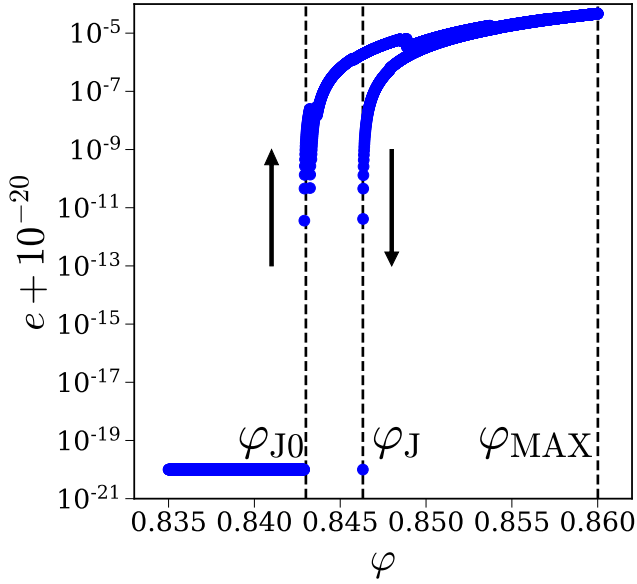


**Fig. 3** The change of the energy during one compression-decompression cycle. The line is shifted by  $10^{-20}$  upward to show the unjammed state points where  $E = 0$ .  $E$  abruptly increasing and it defines  $\varphi_{J0}$  of the poorly trained system and  $E$  vanishes at slightly higher density  $\varphi_J$  on the way back from the training cycle. The position of  $\varphi_{MAX}$  is also shown.

The maximal increase from  $\varphi_J$  for poorly annealed system is about 0.61%, which is comparable with the value reported for the three dimensional system [32]. We then count the number of rattlers in each jammed configuration. We defined the rattler by the particle whose contact number  $Z$  is 0. The green circles in Figure 5 show the total volume fraction of the rattlers  $\varphi_{Rtot}$  as a function of  $\varphi_{MAX}$ . It demonstrates that the rattlers increase as the system is mechanically trained. To quantify the contribution of the particles which maintain the jammed configurations, we define the effective jammed density  $\varphi_J^{eff} = \varphi_J - \varphi_R$  which is plotted in Figure 4 (red square). The result shows that the increase of  $\varphi_J^{eff}$  with  $\varphi_{MAX}$  is far smaller compared with that of  $\varphi_J$ . Compared with 0.61% for  $\varphi_J$ ,  $\varphi_J^{eff}$  increased only by 0.22%, which implies that an increase of  $\varphi_J$  is dominated by the increase of the rattlers. In other literature, the rattler is defined by the particle whose contact number satisfies  $Z < d + 1$  [5]. With this definition,  $\varphi_J^{eff}$  shifts up by about 0.002 but the qualitative behavior is not altered.

We also compare this result with that of a thermally annealed system. We adopt the polydisperse system because it is much easier to equilibrate the system at very high densities using an efficient swap Monte Carlo simulation, than that of binary systems [45]. We use the 22% polydisperse systems with the diameter distribution given by  $P(\sigma) \propto \sigma^{-4}$ . The ratio of minimum

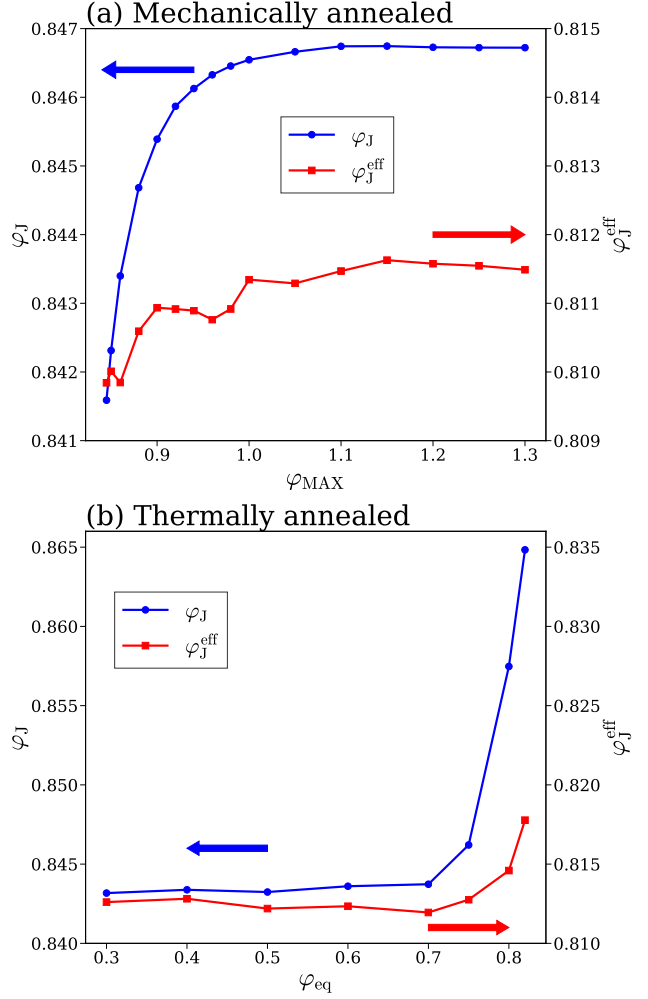


**Fig. 4** (a) The jamming transition point  $\varphi_J$  (the blue circles) and the effective jammed density  $\varphi_J^{eff}$  (the red squares) as a function of  $\varphi_{MAX}$ .  $\varphi_J^{eff}$  is the packing fraction calculated for the particles that contribute to maintain the structure. (b) The same results for the 22% polydisperse harmonic spheres deeply thermally annealed.  $\varphi_{eq}$  is the volume fraction of the parent fluid at a finite  $T = 1.0 \times 10^{-6}$  before quench to generate the jamming configuration.  $\varphi_J$  is constant up to  $\varphi_{eq} \approx 0.7$  and then sharply spike about 3% at  $\varphi_{eff} = 0.82$ . The scales of each axis of the two-axis plot (a) and (b) are aligned.

and the maximum diameter is given by  $\sigma_{min}/\sigma_{max} = 0.45$  [46]. We equilibrate the system of  $N = 1024$  for various densities  $\varphi_{eq}$  at a finite temperature  $T_{eq} = 1.0 \times 10^{-6}$  and then quench the system to  $T = 0$ . The results are insensitive to  $T_{eq}$  as long as it is low enough and  $\varphi_{eq}$  is not large, where the thermodynamic properties of harmonic discs are well approximated by those of hard discs. In Figure 4 (b), we show  $\varphi_J$  (blue circles) and  $\varphi_J^{eff}$  (red squares). As the equilibrium density  $\varphi_{eq}$  increases,  $\varphi_J$  bends upward sharply  $\varphi_{eq} \approx 0.7$ . The position of the bent in our data is close to the mode-coupling transition point  $\varphi_{MCT} = 0.795$  reported in Ref. [46] for a system similar to ours (except for a dif-

ferent polydispersity). The increase of  $\varphi_J^{\text{eff}} = \varphi_J - \varphi_R$  synchronizes with that of  $\varphi_J$  but the degree of the increase is far milder than  $\varphi_J$ , similarly with the result of compression training. This means that the rattlers are primarily responsible for the increase of the jamming packing. This is somewhat surprising because the

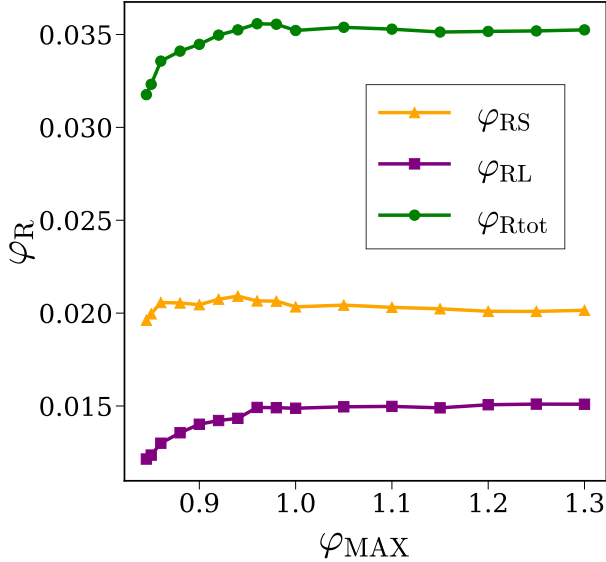


**Fig. 5** The dependence of the volume fraction of total rattler  $\varphi_R$  (green circles), small rattlers  $\varphi_{\text{RS}}$  (yellow triangles), and large rattlers  $\varphi_{\text{RL}}$  (purple square) on the maximal compression  $\varphi_{\text{MAX}}$ . The amplitude of increase of  $\varphi_R$  on  $\varphi_{\text{MAX}}$  is larger than  $\varphi_{\text{RS}}$ . Thus, increase of  $\varphi_R$  is dominant contribution of  $\varphi_{\text{Rtot}}$ .

denser amorphous packing with both thermal annealing and mechanical training is the consequence of the system finds a more stable configuration by descending to the lower entropy landscapes marked by the mode-coupling crossover, which is described by the mean-field picture, whereas the rattlers are objects which is not prescribed by the mean-field scenario.

More surprising is that the large rattlers predominantly contributes to the increase of the jamming density. Figure 5 shows the dependence of the volume fractions of total rattlers  $\varphi_{\text{Rtot}}$ , the rattlers of small discs  $\varphi_{\text{RS}}$ , and of large discs  $\varphi_{\text{RL}}$  on  $\varphi_{\text{MAX}}$  for the mechanical trained binary mixture. Note that the increase of the rattler volume fraction  $\varphi_R$  is dominated by the increase of the large rattlers  $\varphi_{\text{RL}}$  and the number of the small rattlers remains almost constant. Figure 6 is the snapshot of the jammed configurations of (a) poorly trained system and (b) mechanically trained system. Except for the slight decrease of free-area (blank regions) for the denser packing in (b), it is difficult to spot any qualitative changes due to the increase of the large rattlers. It is not clear how the large rattlers contribute to the effi-

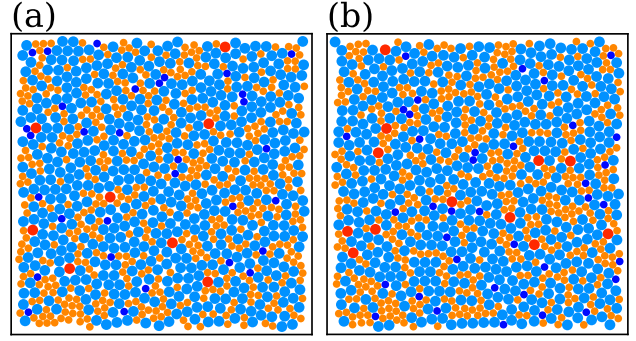


**Fig. 6** The snapshot of the jammed configurations for the poorly trained system (a) and for the trained system with  $\varphi_{\text{MAX}} = 0.98$  (b). The Jamming transition points of these samples are  $\varphi_J = 0.840$  for the poorly trained system and  $\varphi_J = 0.846$  for the trained system with  $\varphi_{\text{MAX}} = 0.98$ . The small rattlers (the blue disks) and the large rattlers (the red disks) are randomly embedded in the non-rattlers of the small (orange disks) and large (light blue disks) disks but the change is barely discernible.

ciency of the packing. We need more quantitative analysis, such as the spatial correlation of the rattlers for a larger system size to dissolve this conundrum [5, 47].

## 4.2 Hyperuniformity

Next we investigate hyperuniformity of the mechanically trained system by compression at the jamming transition point  $\varphi_J$ . We use the  $q$ -dependent compressibility  $\chi(q)$  defined by Eq. (2) to monitor hyperuniformity.

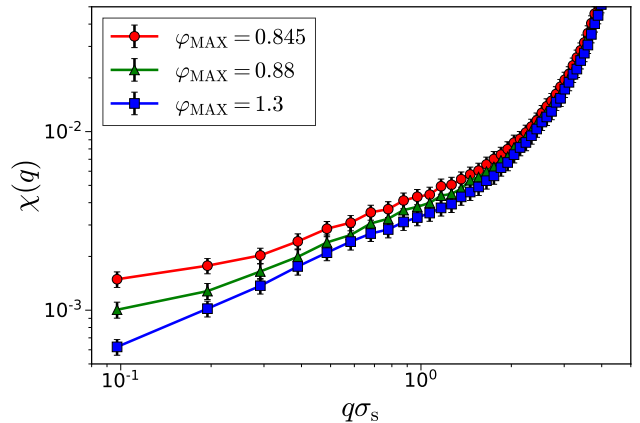


**Fig. 7**  $\chi(q)$  for various  $\varphi_{\text{MAX}}$ .  $q$  is scaled by  $\sigma_s$ . The algebraic decay becomes stronger with increasing the strength of mechanical annealing  $\varphi_{\text{MAX}}$ . Moreover, the intermediate window which emerges hyperuniformity moves lower  $q$  with increasing  $\varphi_{\text{MAX}}$ .

We evaluate  $\chi(q)$  for jammed configurations generated after one cycle of compression-decompression with



various  $\varphi_{\text{MAX}}$ 's. We take the ensemble average of over 300 samples for each  $\varphi_{\text{MAX}}$ . The  $q$ -dependence of  $\chi(q)$  is shown in Figure 7. For all  $\varphi_{\text{MAX}}$ 's, we observe the algebraic behavior of  $\chi(q) \sim q^\alpha$  at the intermediate window of  $0.3 \lesssim q \lesssim 1.3$ . The result of least annealed system ( $\varphi_{\text{MAX}}=0.845$ ) is identical to Figure 1 for which the hyperuniformity exponent is  $\alpha \approx 0.63$ . For larger  $\varphi_{\text{MAX}}$ 's, one observes slight but distinct changes in the behavior of  $\chi(q)$ ; the hyperuniformity exponent  $\alpha$  systematically increases. We plot the dependence of  $\alpha$  on  $\varphi_{\text{MAX}}$  in Figure 8 (green triangles).  $\varphi_J$  (red circles) are plotted on the same figure to highlight the similarity. The exponent  $\alpha$  is obtained by fitting in the region where the algebraic behaviors are observed. The fitting windows are  $0.3 \lesssim q \lesssim 1.3$  for  $0.845 \lesssim \varphi_{\text{MAX}} \lesssim 0.9$  and  $0.1 \lesssim q \lesssim 1.0$  for  $0.9 < \varphi_{\text{MAX}}$ . We observe that the

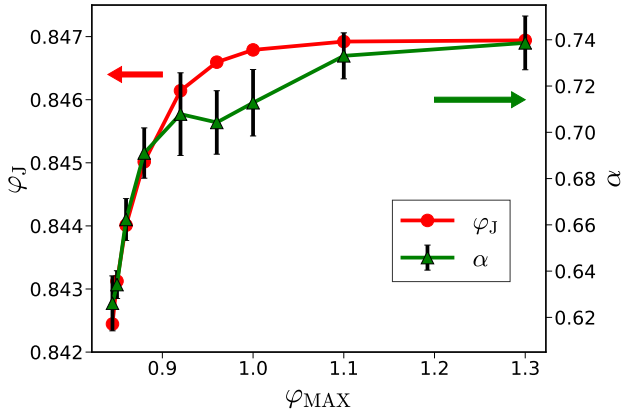


**Fig. 8** The dependence of  $\alpha$  on  $\varphi_{\text{MAX}}$  and  $\varphi_J$ .  $\alpha$  sharply increases as increasing  $\varphi_{\text{MAX}}$  and reaches to  $\alpha \approx 0.74$  at  $\varphi_{\text{MAX}} \approx 1.3$ . This increase of  $\alpha$  on  $\varphi_{\text{MAX}}$  shows similar behavior of  $\varphi_J$ .

increase of  $\alpha$  is similar to that of  $\varphi_J$ , except for a small decrease around  $\varphi_{\text{MAX}} \approx 0.95$ . At  $\varphi_{\text{MAX}} \approx 0.95$ , we observed the effective jammed density  $\varphi_J^{\text{eff}}$  decreases in Figure 4. This hints a correlation between the number of rattler particles and the hyperuniform scaling and worth further investigations. The maximal value of  $\alpha$  at the largest  $\varphi_{\text{MAX}}$  we studied is  $\alpha \approx 0.739 \pm 0.012$ . The increase of  $\alpha$  implies the suppression of the density fluctuations of  $\langle \delta \rho^2(R) \rangle$ . If the argument given in Section 3 holds, the system size dependence of the width of the distributions of the jamming density should become stronger for the mechanically trained system. It is natural to expect that the increase of  $\alpha$  should be observed also for thermally annealed systems. In a recent study, Chieco *et al.* [37] has investigated hyperuniformity of a two-dimensional mixture for jammed packing generated at very low temperatures. Though it is not explicitly mentioned therein, their results hint that the exponent

$\alpha$  faintly larger than those of quickly quenched systems, which is similar to our observation. The fact that  $\alpha$  reaches 0.75 and does not increase further with  $\varphi_{\text{MAX}}$  implies that there exists the upper limit in the effect of the mechanical training. As it is established in the study of nonlinear rheology of the oscillatory sheared systems [48–50], mechanical training plays a similar role as thermal annealing. The system descends the energy landscapes to reach stable configurations by the training. However, there is a maximal shear strain beyond which the system cannot be stabilized anymore. Our results for the compression training seem to be consistent with this argument. We remark that if we apply the compression-decompression cycle more than once,  $\alpha$  also increases with  $\varphi_J$ . In this case,  $\varphi_J$  increases from 0.8469 to 0.8481 and  $\alpha$  increases from  $\alpha = 0.72 \pm 0.02$  to  $\alpha = 0.79 \pm 0.02$  with  $\varphi_{\text{MAX}} = 1.0$  and the number of the training cycle is 50.

Another subtle but possibly important change by the mechanical training observed in Figure 7 is that the window in which hyperuniformity is observed widens slightly as  $\varphi_{\text{MAX}}$  increases. In other words, the cut-off wavevector, or the inverse of the hyperuniform length,  $q_{\text{HU}}$ , below which  $\chi(q)$  bends up, becomes smaller. This may be the consequences of the stabilization of the jamming configurations by mechanical training, which is consistent with the argument in Ref. [28] that the ideal hyperuniformity with  $\chi(q) \rightarrow 0$  as  $q \rightarrow 0$  is realized only in the ideally stable configurations. However, the changes are too small to be conclusive. We leave more systematic analysis using the larger systems and with different training/annealing protocols for future work.

## 5 Hyperuniformity of oscillatory sheared systems below the jamming transition point

In this section, we turn our attention to the system below the jamming transition point and study the geometrical properties of the configurations under mechanical training. Instead of compression, we apply the quasi-static oscillatory shear to the system.

The athermal and periodically driven systems attract much attention recently in the context of the nonequilibrium phase transition in the dilute regime far below the jamming transition point [23, 52–54]. When periodically sheared, the athermal particles originally distributed randomly move with the shear flow, collide with other particles, and then redistribute after collisions. If the amplitude of the shear cycle,  $\gamma$ , is small, the particles find the optimal configurations after multiple oscillatory shear cycles, in which all particles return to the same positions after every cycle. If  $\gamma$  exceeds a threshold value  $\gamma_c$ , the particles never come back to the

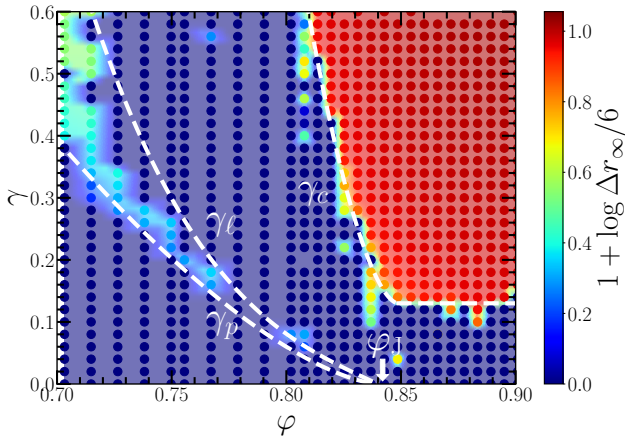


**Fig. 9** The nonequilibrium phase diagram of the reversible-irreversible phase transition in the vicinity of the jamming point. The heat map of the average particle displacement per oscillation cycle in the stationary state,  $\Delta r_\infty$  is plotted in the  $(\varphi, \gamma)$ -plane [51]. The  $\gamma_p$  and  $\gamma_\ell$  lines separate the point-reversible phase, quasi-irreversible phase, and the loop-reversible phase, respectively.  $\gamma_c$  represents the reversible-irreversible transition line. The white-broken lines are guides for the eyes.

original positions and start diffusing over the space. It is called the reversible-irreversible (RI) transition and this transition is now believed to belong to universality class either of the directed percolation or conserved directed percolation (Manna) classes [55]. Furthermore, the density fluctuations are suppressed and the system becomes hyperuniform near the transition point. The spectrum exhibits a power-law behavior  $\chi(q) \sim q^\alpha$  at small wavevectors with a universal exponent  $\alpha \approx 0.45$  for  $d = 2$  [23, 53, 54]<sup>2</sup> and  $\alpha \approx 0.25$  for  $d = 3$  [56]. The hyperuniformity of the RI transition is also studied in a different experimental setup [57].

A natural question is how the nature of the RI transition at low-density regime changes if the density is below but close to the jamming transition point. Recently, the RI transition in the vicinity of  $\varphi_J$  has been studied under the quasi-static oscillatory shear cycles in both  $d = 2$  [51, 58] and  $d = 3$  [59, 60] slightly below and slightly above  $\varphi_J$  [61]. Above  $\varphi_J$ , the RI transition point  $\gamma_c$  is almost identical with the yielding transition point  $\gamma_Y$  [62], which is natural as the microscopic trajectories of particles would be reversible in the elastic region and the trajectories become diffusive beyond the yielding transition point where the system is fluidized. The exception is the critical region close to  $\varphi_J$  where the elastic response becomes nonlinear [16, 63].

The nature of the RI transition slightly below  $\varphi_J$  is far richer. The  $\gamma_c$ -line suddenly increases as  $\varphi$  de-

parts below  $\varphi_J$  (see Figure 9).  $\gamma_c$ , however, is not vertical against  $\varphi$  at  $\varphi_J$ . The irreversible phase seeps into  $\varphi < \varphi_J$  and the large  $\gamma$  region. Interestingly, the microscopic and short-range structures of particles along the  $\gamma_c$ -lines below  $\varphi_J$  are very similar to those of the jammed configurations of the frictional particles [59]. The reversible phase well below  $\gamma_c$  is also unique in this density regime [51, 58]. If  $\gamma$  is small enough, the trajectory of particles per cycle in the stationary state is characterized by a straight line formed by a shear convection, as the particles experience no collision with others on the way forward and backward during one shear-cycle. We refer to this phase as the point-reversible phase since the non-affine trajectories of the particles are just points. As  $\gamma$  increases beyond a threshold value,  $\gamma_p$ , the trajectories do not converge to a stationary state within the simulation time windows. At larger  $\gamma = \gamma_\ell$ , the trajectories become reversible again, but the nature of the trajectories change qualitatively. The particles experience multiple collisions and those particles experience jaggy trajectories before traveling back to the original positions per shear-cycle. This phase exists until  $\gamma$  crosses  $\gamma_c$ , beyond which the trajectories become irreversible. We call the phase between  $\gamma_\ell \leq \gamma \leq \gamma_c$  the loop-reversible phase.  $\gamma_\ell$  is well below  $\gamma_c$  and it converges to 0 as  $\varphi$  approaches  $\varphi_J$ .

The relaxation “time”,  $\tau_c$ , which is defined by the number of oscillatory cycles required for the system to reach the stationary state increases sharply as  $\gamma$  approaches  $\gamma_p$  [51, 58] and the order parameter such as the fraction of the irreversible particles or the average particle displacement per cycle  $\Delta r_\infty$  in the stationary state seems to increase continuously, in the stark contrast with the RI transition at  $\gamma_c$ , where  $\Delta r_\infty$  jump from zero to a finite value discontinuously. We reported that there is a narrow strip of the irreversible phase just above  $\gamma_p$  in the previous study [51], where the particles never reach the reversible state and thus  $\Delta r_\infty$  remains small but finite (see the narrow region between the  $\gamma_p$  and  $\gamma_\ell$  lines in Figure 9). It may be a natural consequence of the diverging relaxation time which exceeds the simulation time windows. But close inspections of the loop trajectories indicate that the particles keep migrating over many cycles with little sign to relax to a stationary state. The nature of this peninsula is still elusive and we shall name the region as the quasi-irreversible phase. Due to these complexities, the identification of the precise position of the transition is challenging, which is the reason why the  $\gamma_p$  and  $\gamma_\ell$  lines in Figure 9 are not sharply defined.

We investigate the density fluctuations in the vicinity of this point-to-loop transition point  $\gamma_p$  for the two-dimensional binary mixture. In the simulation, we fix

<sup>2</sup>Tjhung *et al.* argued that  $\alpha$  crosses over to 1 at very small  $q$  [23].



the density at  $\varphi = 0.82$ , slightly below  $\varphi_J \approx 0.842$ . Note that, at this density, the irreversible phase was not clearly observed and  $\gamma_p \approx \gamma_\ell$ . The box size is  $L = 42$  and the number of samples is from 300 to 900, depends on  $\gamma$ . We place the system under quasi-static oscillatory shear of various amplitudes  $\gamma$ . In the quasi-static shear protocol, the system is deformed by the small shear  $|\Delta\gamma| = 10^{-3}$  incrementally. At each incremental step, the system's configuration is relaxed by FIRE algorithm [35]. Note that in the FIRE algorithm, the finite mass is endowed to every particle and the trajectories towards the energy minima always overrun slightly due to the inertia, which inevitably enhances the chance for the particles to collide with others during the minimization processes. Thus, the particles' position after one shear cycle shifts slightly from the original position. We still use the FIRE algorithm instead of the conventional steepest descent method because it is far faster and computationally cheaper than the latter. We carefully checked the configurations generated by both algorithms and found that the difference is negligible as long as the density fluctuations are concerned.

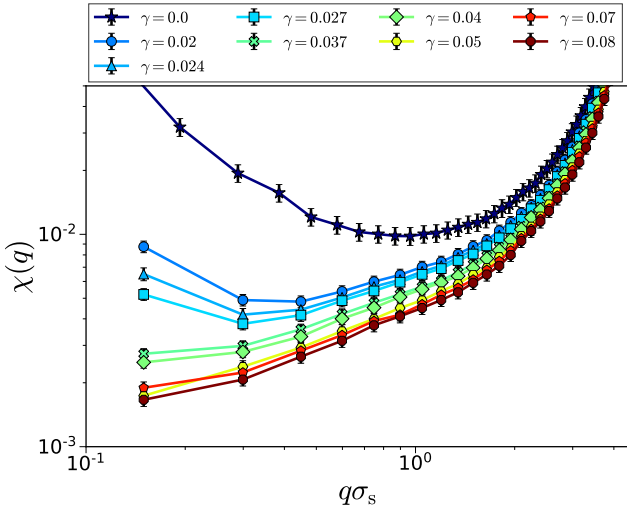


**Fig. 10**  $\chi(q)$  for various shear amplitude  $\gamma$  at  $\varphi = 0.82$ . At this density, the transition from the point to loop reversible phase takes place around  $\gamma_p \approx 0.04$ .

Figure 10 shows  $\chi(q)$  defined by Eq. (2) for  $\gamma = 0 \sim 0.08$ . Note that  $\gamma_p \approx 0.04$  at this density. When  $\gamma = 0$ , no sign of hyperuniformity is observed.  $\chi(q)$  goes up at small  $q$ , reflecting that the particles' configuration is random and it tends to obey the Poissonian statistics for which  $\chi(q \rightarrow 0) = 1$ . However, as  $\gamma$  increases, the upward bends are gradually suppressed. Eventually, the line converges to a single curve which is algebraic. This convergence takes place around  $\gamma \approx 0.05$ , which is very close to  $\gamma_p$ . Surprisingly, the exponent of the curve

$\chi(q) \sim q^\alpha$  is  $\alpha \approx 0.642 \pm 0.014$  at  $\gamma = 0.05$ . This exponent is close to that of the poorly trained system discussed in Section 3.

We plot the  $\gamma$ -dependence of  $\alpha$  in Figure 11.  $\alpha$ 's are extracted by fitting by power-laws for the wavevector windows whose size varies depending on  $\gamma$ 's. At small  $\gamma$  regime, the fitting is less trustworthy because the power-law windows are narrow, if they exists. Sur-

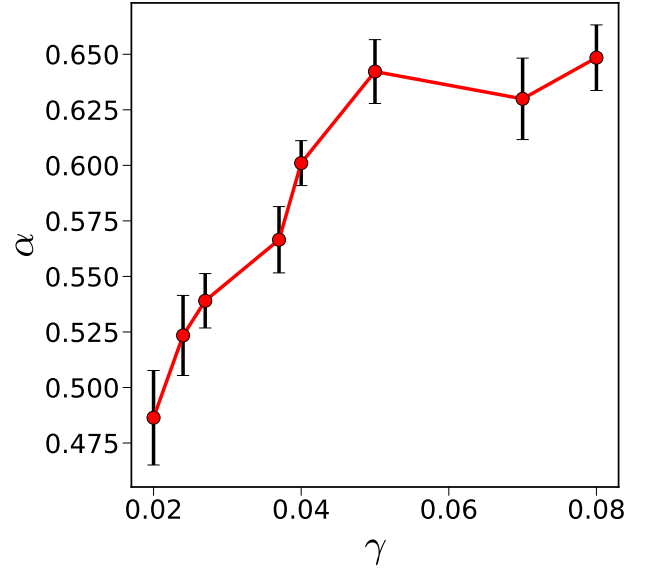


**Fig. 11**  $\gamma$ -dependence of  $\alpha$ .  $\alpha$  monotonically increases with  $\gamma$  up to  $\gamma = 0.05$ . This value is close to  $\gamma_p \approx 0.04$  at  $\varphi = 0.82$ .

prisingly,  $\alpha$  becomes constant at large  $\gamma$  and hyperuniformity persists well above the point-to-loop transition point,  $\gamma_p$ . This result is in stark contrast with the RI phase transition in the dilute regime where hyperuniformity is observed only in the close vicinity of the transition point,  $\gamma_c$ . We emphasize that hyperuniformity observed here is distinct from that observed for a similar density window but at a much larger shear amplitude near  $\gamma_c (\gg \gamma_p)$ , where the discontinuous RI transition is observed [60]. Their exponent for the system under the strong oscillatory shear in  $d = 3$  was  $\alpha \approx 0.45$ . The result in Figure 10, on the other hand, demonstrates that the sheared system with very small perturbation inherits the geometrical properties of the configuration exactly at the jamming point. Contrary to the system trained by compression at  $\varphi > \varphi_J$ , the exponent  $\alpha$  remains constant for large amplitude beyond  $\gamma_p$ . Here we studied only one density  $\varphi = 0.82$ . It is important to check whether this hyperuniform behavior near the jamming transition crosses over to that near the DP universality class at very low densities, where  $\alpha \approx 0.45$ .

## 6 Summary

In this paper, we shed light on the several facets of the geometrical properties of the jammed or nearly jammed configurations of a two-dimensional binary mixture of particles with harmonic potential under nonequilibrium perturbation. We primarily focused on hyperuniformity of the system by monitoring the wavevector dependent compressibility  $\chi(q)$  defined by Eq. (2). We first revisited hyperuniformity of unperturbed jammed configuration. The observation of  $\chi(q) \sim q^\alpha$  with the exponent of  $\alpha \approx 0.63$  for  $d = 2$  instead of  $\alpha \approx 1$  for the three-dimensional counterparts seems to be unnoticed to the best of our knowledge, though the data reported in the literature is consistent with those shown in Figure 1. We then placed the jammed configurations under a compression cycle from  $\varphi < \varphi_{J0}$  to  $\varphi = \varphi_{\text{MAX}}$ .  $\varphi_J$  after this training cycle is slightly larger than  $\varphi_{J0}$  of the poorly trained system. We found that the number of rattlers increased as  $\varphi_J$  increase. This result indicates that the increases of  $\varphi_J$  do not lead to the increase of the packing fraction of particles that sustain the force network of the jammed structures. We also find that the larger particles are responsible for the increase in the number of rattlers. It is puzzling because our intuition tells us that the large particles would be easier to form the contact networks in a more stable configuration than the smaller ones which would tend to find themselves in the free volume pockets. More analysis of the system size dependence and the detailed microscopic studies on the spatial correlations of the rattlers are necessary to resolve this conundrum. Another finding is that the exponent of hyperuniformity  $\alpha$  increases with  $\varphi_{\text{MAX}}$  from  $\alpha \approx 0.63$  up to as large as  $\alpha \approx 0.74$ . The value does not increase beyond this value with larger  $\varphi_{\text{MAX}}$ . Since mechanical training plays similar roles as thermal annealing, our results imply that the suppression of the density fluctuations should be observed for the jammed configurations generated from the thermally annealed fluids. Furthermore, the wavevector  $q_{\text{HU}}$ , the inverse of the hyperuniform length, below which  $\chi(q)$  ceases to decrease and bends upward also tends to shift to lower values. The results shown in Figure 7 are not conclusive but this may suggest that hyperuniformity extends to the large length scales as the system is more trained and finds more stable configurations. This is consistent with the scenario proposed by Godfrey *et al.* [28].

We also expect to observe qualitatively similar results when the system is cyclically sheared instead of the compression cycles above  $\varphi_J$ . Recently, Das *et al.* [61] have shown that  $\varphi_J$  increases under the quasi-static oscillatory shear when the shear strain amplitude is small, much the same way that  $\varphi_J$  increases with the compres-

sion cycle. It would be interesting to study hyperuniformity along  $\varphi_J$ -line, which increases with the shear amplitude  $\gamma$  and see if the exponent  $\alpha$  increases and  $q_{\text{HU}}$  decreases with the shear training [64]. In Section 5, we have carried out the quasi-static oscillatory shear experiment at  $\varphi = 0.82$  that is below  $\varphi_J = 0.842$ . The system is not hyperuniform when  $\gamma = 0$ , but as the shear amplitude increases, the large-scale density fluctuations becomes suppressed gradually and eventually become hyperuniform with the same exponent  $\alpha \approx 0.64$  as the poorly trained configuration at the jamming transition point  $\varphi_J$ . The convergence to hyperuniform state takes place when  $\gamma$  crosses the transition point  $\gamma_p \approx \gamma_\ell$ . Hyperuniformity observed here is distinct from that observed at the reversible-to-irreversible transition point  $\gamma_c$  at larger  $\gamma$  [59, 60]. Figure 9 hints that the  $\gamma_c$ -line near the jamming transition point does not extrapolate and connect smoothly to the RI transition line at the low density limit, where the *bona fide* nonequilibrium transition of the DP (or Manna) universality classes are expected. Connecting the RI transition lines at the two disparate density regions are important future work.

In this paper, we displayed the results only for a few representative state points with moderate system sizes. All mechanical perturbation used here is quasi-static protocols and requires heavy computational loads as well as many samplings to obtain the good statistics. Exploring systematically more state points with larger system sizes will be necessary to reveal the whole pictures of the rich and anomalous geometrical properties of the nonequilibrium configuration near the jamming transition point.

**Acknowledgements** Discussion with Srikanth Sastry and Misaki Ozawa is very fruitful. This work was financially supported by KAKENHI Grants 18H01188, 19H01812, 19K03767, 20H05157, and 20H00128.

## References

1. A.J. Liu, S.R. Nagel, Jamming is not just cool any more, *Nature* **396**(6706), 21 (1998)
2. A.J. Liu, S.R. Nagel, W. van Saarloos, M. Wyart, in *Dynamical heterogeneities in glasses, colloids, and granular media*, ed. by L. Berthier, G. Biroli, J.P. Bouchaud, L. Cipeletti, W. van Saarloos (Oxford University Press, 2010)
3. M. van Hecke, Jamming of soft particles: geometry, mechanics, scaling and isostaticity, *Journal of Physics: Condensed Matter* **22**(3), 033101 (2010)
4. G. Parisi, P. Urbani, F. Zamponi, *Theory of Simple Glasses: Exact Solutions in Infinite Dimensions* (Cambridge University Press, Cambridge, 2020)

5. M. Ozawa, L. Berthier, D. Coslovich, Exploring the jamming transition over a wide range of critical densities, *SciPost Phys.* **3**, 027 (2017)
6. P. Charbonneau, J. Kurchan, G. Parisi, P. Urbani, F. Zamponi, Glass and jamming transitions: From exact results to finite-dimensional descriptions, *Annual Review of Condensed Matter Physics* **8**(1), 265 (2017)
7. C.S. O'Hern, L.E. Silbert, A.J. Liu, S.R. Nagel, Jamming at zero temperature and zero applied stress: The epitome of disorder, *Phys. Rev. E* **68**, 011306 (2003)
8. M. Wyart, S.R. Nagel, T.A. Witten, Geometric origin of excess low-frequency vibrational modes in weakly connected amorphous solids, *Europhysics Letters (EPL)* **72**(3), 486 (2005)
9. H. Mizuno, H. Shiba, A. Ikeda, Continuum limit of the vibrational properties of amorphous solids, *Proceedings of the National Academy of Sciences* **114**(46), E9767 (2017)
10. Y. Jin, P. Urbani, F. Zamponi, H. Yoshino, A stability-reversibility map unifies elasticity, plasticity, yielding, and jamming in hard sphere glasses, *Science Advances* **4**(12) (2018)
11. A. Ikeda, T. Kawasaki, L. Berthier, K. Saitoh, T. Hatano, Universal relaxation dynamics of sphere packings below jamming, *Phys. Rev. Lett.* **124**, 058001 (2020)
12. K. Saitoh, T. Hatano, A. Ikeda, B.P. Tighe, Stress relaxation above and below the jamming transition, *Phys. Rev. Lett.* **124**, 118001 (2020)
13. D. Vågberg, P. Olsson, S. Teitel, Critical scaling of bagnold rheology at the jamming transition of frictionless two-dimensional disks, *Phys. Rev. E* **93**, 052902 (2016)
14. J. Boschan, D. Vågberg, E. Somfai, B.P. Tighe, Beyond linear elasticity: Jammed solids at finite shear strain and rate, *Soft Matter* **12**(24), 5450 (2016)
15. T. Kawasaki, D. Coslovich, A. Ikeda, L. Berthier, Diverging viscosity and soft granular rheology in non-brownian suspensions, *Phys. Rev. E* **91**, 012203 (2015)
16. M. Otsuki, H. Hayakawa, Avalanche contribution to shear modulus of granular materials, *Phys. Rev. E* **90**, 042202 (2014)
17. C. Brito, H. Ikeda, P. Urbani, M. Wyart, F. Zamponi, Universality of jamming of nonspherical particles, *Proceedings of the National Academy of Sciences* (2018)
18. S. Torquato, F.H. Stillinger, Local density fluctuations, hyperuniformity, and order metrics, *Phys. Rev. E* **68**, 041113 (2003)
19. S. Torquato, Hyperuniform states of matter, *Physics Reports* **745**, 1 (2018)
20. A. Gabrielli, M. Joyce, F. Sylos Labini, Glass-like universe: Real-space correlation properties of standard cosmological models, *Phys. Rev. D* **65**, 083523 (2002)
21. Y. Jiao, T. Lau, H. Hatzikirou, M. Meyer-Hermann, J.C. Corbo, S. Torquato, Avian photoreceptor patterns represent a disordered hyperuniform solution to a multiscale packing problem, *Phys. Rev. E* **89**, 022721 (2014)
22. Q.L. Lei, M.P. Ciamarra, R. Ni, Nonequilibrium strongly hyperuniform fluids of circle active particles with large local density fluctuations, *Science Advances* **5**(1), eaau7423 (2019)
23. E. Tjhung, L. Berthier, Criticality and correlated dynamics at the irreversibility transition in periodically driven colloidal suspensions, *Journal of Statistical Mechanics: Theory and Experiment* **2016**(3), 033501 (2016)
24. J.H. Weijs, R. Jeanneret, R. Dreyfus, D. Bartolo, Emergent hyperuniformity in periodically driven emulsions, *Phys. Rev. Lett.* **115**, 108301 (2015)
25. A. Donev, S. Torquato, F.H. Stillinger, Pair correlation function characteristics of nearly jammed disordered and ordered hard-sphere packings, *Phys. Rev. E* **71**, 011105 (2005)
26. A. Ikeda, L. Berthier, Thermal fluctuations, mechanical response, and hyperuniformity in jammed solids, *Phys. Rev. E* **92**, 012309 (2015)
27. A. Ikeda, L. Berthier, G. Parisi, Large-scale structure of randomly jammed spheres, *Phys. Rev. E* **95**, 052125 (2017)
28. M.J. Godfrey, M.A. Moore, Absence of hyperuniformity in amorphous hard-sphere packings of non-vanishing complexity, *Phys. Rev. Lett.* **121**, 075503 (2018)
29. Y. Zheng, Y.W. Li, M.P. Ciamarra, Hyperuniformity and density fluctuations at a rigidity transition in a model of biological tissues, *Soft Matter* **16**, 5942 (2020)
30. S. Mitra, A.D.S. Parmar, P. Leishangthem, S. Sastry, G. Foffi, Hyperuniformity in cyclically driven glasses, *Journal of Statistical Mechanics: Theory and Experiment* **2021**(3), 033203 (2021)
31. Y. Yuan, Y. Jiao, Y. Wang, S. Li, Universality of jammed frictional packing, *Phys. Rev. Research* **3**, 033084 (2021)
32. N. Kumar, S. Luding, Memory of jamming—multiscale models for soft and granular matter, *Granular Matter* **18**(3), 58 (2016)
33. P. Chaudhuri, L. Berthier, S. Sastry, Jamming transitions in amorphous packings of frictionless spheres

- occur over a continuous range of volume fractions, *Phys. Rev. Lett.* **104**, 165701 (2010)
34. M. Ozawa, T. Kuroiwa, A. Ikeda, K. Miyazaki, Jamming transition and inherent structures of hard spheres and disks, *Phys. Rev. Lett.* **109**, 205701 (2012)
  35. E. Bitzek, P. Koskinen, F. Gähler, M. Moseler, P. Gumbsch, Structural relaxation made simple, *Phys. Rev. Lett.* **97**, 170201 (2006)
  36. Y. Wu, P. Olsson, S. Teitel, Search for hyperuniformity in mechanically stable packings of frictionless disks above jamming, *Phys. Rev. E* **92**, 052206 (2015)
  37. A.T. Chieco, M. Zu, A.J. Liu, N. Xu, D.J. Durian, Spectrum of structure for jammed and unjammed soft disks, *Phys. Rev. E* **98**, 042606 (2018)
  38. L. Berthier, P. Chaudhuri, C. Coulais, O. Dauchot, P. Sollich, Suppressed compressibility at large scale in jammed packings of size-disperse spheres, *Phys. Rev. Lett.* **106**, 120601 (2011)
  39. T. Kawasaki, K. Miyazaki, Shear jamming and shear melting in mechanically trained frictionless particles, , arXiv:2003.10716
  40. R. Dreyfus, Y. Xu, T. Still, L.A. Hough, A.G. Yodh, S. Torquato, Diagnosing hyperuniformity in two-dimensional, disordered, jammed packings of soft spheres, *Phys. Rev. E* **91**, 012302 (2015)
  41. D. Hexner, A.J. Liu, S.R. Nagel, Two diverging length scales in the structure of jammed packings, *Phys. Rev. Lett.* **121**, 115501 (2018)
  42. C.E. Zachary, Y. Jiao, S. Torquato, Hyperuniform long-range correlations are a signature of disordered jammed hard-particle packings, *Phys. Rev. Lett.* **106**, 178001 (2011)
  43. K. Binder, M. Nauenberg, V. Privman, A.P. Young, Finite-size tests of hyperscaling, *Phys. Rev. B* **31**, 1498 (1985)
  44. D. Hexner, P. Urbani, F. Zamponi, Can a large packing be assembled from smaller ones?, *Phys. Rev. Lett.* **123**, 068003 (2019)
  45. A. Ninarello, L. Berthier, D. Coslovich, Models and algorithms for the next generation of glass transition studies, *Phys. Rev. X* **7**, 021039 (2017)
  46. Q. Liao, L. Berthier, Hierarchical landscape of hard disk glasses, *Phys. Rev. X* **9**, 011049 (2019)
  47. S. Atkinson, F.H. Stillinger, S. Torquato, Detailed characterization of rattlers in exactly isostatic, strictly jammed sphere packings, *Phys. Rev. E* **88**, 062208 (2013)
  48. A.D.S. Parmar, S. Kumar, S. Sastry, Strain localization above the yielding point in cyclically deformed glasses, *Phys. Rev. X* **9**, 021018 (2019)
  49. W.T. Yeh, M. Ozawa, K. Miyazaki, T. Kawasaki, L. Berthier, Glass stability changes the nature of yielding under oscillatory shear, *Phys. Rev. Lett.* **124**, 225502 (2020)
  50. H. Bhaumik, G. Foffi, S. Sastry, The role of annealing in determining the yielding behavior of glasses under cyclic shear deformation, *Proceedings of the National Academy of Sciences* **118**(16) (2021)
  51. K. Nagasawa, K. Miyazaki, T. Kawasaki, Classification of the reversible-irreversible transitions in particle trajectories across the jamming transition point, *Soft Matter* **15**, 7557 (2019)
  52. L. Corte, P.M. Chaikin, J.P. Gollub, D.J. Pine, Random organization in periodically driven systems, *Nature Physics* **4**(5), 420 (2008)
  53. D. Hexner, D. Levine, Hyperuniformity of critical absorbing states, *Phys. Rev. Lett.* **114**, 110602 (2015)
  54. Y. Zheng, A.D.S. Parmar, M. Pica Ciamarra, Hidden order beyond hyperuniformity in critical absorbing states, *Phys. Rev. Lett.* **126**, 118003 (2021)
  55. S. Lübeck, Universal scaling behavior of nonequilibrium phase transitions., *International Journal of Modern Physics B: Condensed Matter Physics; Statistical Physics; Applied Physics* **18**(31/32), 3977 (2004)
  56. S. Wilken, R.E. Guerra, D.J. Pine, P.M. Chaikin, Hyperuniform structures formed by shearing colloidal suspensions, *Phys. Rev. Lett.* **125**, 148001 (2020)
  57. J. Wang, J. Schwarz, J.D. Paulsen, Hyperuniformity with no fine tuning in sheared sedimenting suspensions, *Nature communications* **9**(1), 1 (2018)
  58. C.F. Schreck, R.S. Hoy, M.D. Shattuck, C.S. O'Hern, Particle-scale reversibility in athermal particulate media below jamming, *Phys. Rev. E* **88**, 052205 (2013)
  59. H.A. Vinutha, S. Sastry, Disentangling the role of structure and friction in shear jamming, *Nature Physics* **12**(6), 578 (2016)
  60. H.A. Vinutha, S. Sastry, Geometric aspects of shear jamming induced by deformation of frictionless sphere packings, *Journal of Statistical Mechanics: Theory and Experiment* **2016**(9), 094002 (2016)
  61. P. Das, H.A. Vinutha, S. Sastry, Unified phase diagram of reversible-irreversible, jamming, and yielding transitions in cyclically sheared soft-sphere packings, *Proceedings of the National Academy of Sciences* **117**(19), 10203 (2020)
  62. T. Kawasaki, L. Berthier, Macroscopic yielding in jammed solids is accompanied by a nonequilibrium first-order transition in particle trajectories, *Phys. Rev. E* **94**, 022615 (2016)

- 
63. S. Dagois-Bohy, E. Somfai, B.P. Tighe, M. van Hecke, Softening and yielding of soft glassy materials, *Soft Matter* **13**, 9036 (2017)
  64. M. Shukawa, H. Matsuyama, T. Kawasaki, K. Miyazaki, , (unpublished)